Alzheimer's Research & Therapy

RESEARCH

Open Access

Investigating the Aβ and tau pathology in autosomal dominant Alzheimer's disease: insights from hybrid PET/MRI and network mapping

Zhi Zhou[1], Qigeng Wang[2], Linwen Liu[3], Qi Wang[2], Xiaojun Zhang[4], Can Li[4], Jiajin Liu[4], Yidan Wei[5], Jin Gao[5], Liping Fu[5*] and Ruimin Wang[4*]

Abstract

Background Autosomal dominant Alzheimer's disease (ADAD) offers a distinct framework to study the preclinical phase of Alzheimer's disease (AD), due to its predictable symptom onset and high penetrance of causative mutations. The study aims to examine the spatial distribution and temporal progression of amyloid-beta (Aβ) and tau pathologies, along with mapping the pathology-functional connectivity network, in asymptomatic ADAD mutation carriers using hybrid positron emission tomography/magnetic resonance imaging (PET/MRI).

Methods Participants were recruited from the Chinese Familial Alzheimer's Disease Network, comprising 14 asymptomatic ADAD mutation carriers and 20 cognitively normal healthy controls (CN). Aβ deposition was evaluated using ^{11}C-PIB PET, while tau aggregation was assessed via ^{18}F-MK6240 PET imaging. Resting-state functional connectivity (rsFC) was analyzed to investigate relationships between pathological burden and neural network changes. Through qualitative analysis, ADAD carriers with marked ^{18}F-MK6240 uptake in intracranial regions were categorized into Group 2, while others were designated as Group 1.

Results Asymptomatic ADAD carriers demonstrated a significantly greater Aβ burden across the cortex and striatum compared to CN, although tau PET binding did not differ significantly between the groups. Group 2 participants exhibited elevated ^{11}C-PIB uptake in the neocortex and striatum, and increased ^{18}F-MK6240-PET uptake in the medial temporal and other cortical regions. Compared with Group 1, network mapping of rsFC in Group 2 indicated increased connectivity associated with tau deposition in limbic, posterior cortical, and bilateral temporal regions, overlapping with the default mode network, suggesting potential compensatory mechanisms. Additionally, reduced connectivity in the left medial inferior temporal cortex and fusiform gyrus aligned with findings in sporadic AD cases.

Conclusions This study shows the spatiotemporal progression of Aβ and tau pathologies in preclinical ADAD, supporting the hypothesis that Aβ deposition precedes tau pathology. The rsFC alterations observed associate with

*Correspondence:
Liping Fu
flp39@163.com
Ruimin Wang
wrm@yeah.net

Full list of author information is available at the end of the article

tau deposition in asymptomatic carriers indicate early network disruptions. Tau network mapping presents a valuable approach for assessing individualized brain connectivity changes in preclinical AD, mitigating single-subject variability and advancing precision assessment in early-stage AD diagnosis.

Keywords Autosomal dominant Alzheimer's disease, Alzheimer's disease, Amyloid-beta, Tau, Hybrid PET/MRI, Functional connectivity, Rest-state functional MRI

Introduction

Amyloid-beta (Aβ) and tau deposition are hallmark pathologies of Alzheimer's disease (AD), with evidence suggesting that these pathological changes initiate many years before the onset of clinical symptoms [1]. Recently, disease-modifying treatments, including anti-Aβ and anti-tau antibodies, have emerged rapidly, emphasizing the importance of early detection and predicting AD progression during the preclinical phase.

Autosomal dominant Alzheimer's disease (ADAD), driven by mutations in the amyloid precursor protein (APP) and *Presenilin 1/2 (PSEN1/2)* genes [2], provides an ideal model for examining AD pathology in its preclinical stages [2, 3]. ADAD mutation carriers exhibit a predictable age of symptom onset and near-complete mutation penetrance [4]. Furthermore, the younger onset of ADAD minimizes age-related comorbidities, such as cerebrovascular pathology or tau accumulation due to aging, that might otherwise confound neuroimaging studies [5].

Despite these insights, the spatiotemporal patterns of pathology in ADAD and their comparability to sporadic AD remain an area of ongoing investigation. Prior studies have shown that, unlike sporadic AD, ADAD exhibits an atypical distribution of Aβ and tau. In preclinical ADAD, Aβ often accumulates more in the striatum than in the neocortex [6–10], and tau deposition has been detected early in posterior brain regions (e.g., precuneus and posterior cingulate), differing from traditional Braak staging [11]. Another study, however, reported tau spread from the entorhinal cortex to the neocortex, aligning with the typical progression in sporadic AD [12].

Within the A/T/N framework, AD pathology initiates with Aβ accumulation (A), followed by tau aggregation (T), leading ultimately to neurodegeneration (N) [13]. While functional network disconnection is widely recognized as a downstream effect of AD pathology, the mechanisms behind this process are not fully investigated. Evidence suggests that the spread of Aβ and tau disrupts functional networks, leading to neuronal dysfunction, impaired synaptic plasticity, and disrupted neural communication [14–16]. Utilizing hybrid PET/MRI, our previous research found that tau pathology reduces the strength of resting-state functional connectivity (rsFC) in sporadic AD [17]. Understanding the influence of Aβ and tau pathology on neural degeneration in the preclinical stage of AD could be crucial for early diagnosis and therapeutic intervention.

This study recruited asymptomatic ADAD mutation carriers and cognitively normal healthy volunteers (CN) and utilized hybrid PET/MRI to assess the convergence of neurofunctional and pathological alterations. The specific objectives were: (1) to characterize the spatial distribution and temporal dynamics of Aβ and tau pathology in preclinical ADAD using ^{11}C-PIB and ^{18}F-MK6240 PET, and (2) to evaluate the relationship between rsFC and pathological tau deposition. This integrative approach offers valuable insights into the neurobiological mechanisms underlying preclinical AD and potential avenues for targeted early interventions.

Methods

Study design and participants

ADAD participants in this study were recruited from a longitudinal cohort study of the Chinese Familial Alzheimer's Disease Network (CFAN) at Xuanwu Hospital, Beijing. All visits occurred between August 2021 and July 2024. Eligibility criteria included: (i) age 18 or over, (ii) a confirmed family history of ADAD, (iii) being asymptomatic (Mini-Mental State Examination (MMSE) score above 24 and Clinical Dementia Rating (CDR) score of 0) with an inherited pathogenic mutation in *PSENs1/2* or APP genes, predicting symptom onset similar to their affected parent. Exclusion criteria were: (i) structural abnormalities that could lead to dementia, such as cortical infarction, tumors, or a subdural hematoma; (ii) concurrent non-dementia illnesses affecting cognitive function at the time of MRI examination; (iii) metabolic conditions including hypothyroidism, and vitamin B12 or folic acid deficiencies. All participants underwent a standard cognitive battery, comprising: (i) CDR; (ii) MMSE; (iii) Hamilton Depression Scale (HAMD); (iv) WHO-UCLA word memory; and (v) Boston Naming Test. APOE ε4 status was classified as ε4 carriers (ε4+, including heterozygotes and homozygotes) and ε4 non-carriers (ε4-). Estimated years to symptom onset (EYO) for each asymptomatic ADAD carrier was calculated by subtracting the age at which the participant's affected parent first developed progressive cognitive decline from the participant's current age at assessment [11].

CN subjects had no history of neurological or psychiatric disorders, sensorimotor impairments, or cognitive complaints, showed no abnormalities on brain MRI, and

exhibited no cognitive deficits on neuropsychological testing. All participants provided informed written consent before enrollment, and the study was approved by the institutional review board of the Chinese PLA General Hospital. We conducted this study in compliance with the principles of the Declaration of Helsinki.

Radiosynthesis of ^{18}F-MK6240 and ^{11}C-PIB

^{18}F-MK6240 was synthesized using a di-Boc-protected nitro precursor in the presence of Tetrabutylammonium bicarbonate (TBA-HCO_3) on an automated synthesis module (PET-MF-2 V-IT-1, Beijing, China). After azeotropic drying, radiofluorination coupled with Boc deprotection was conducted by heating the reaction to 165 °C for 15 min under mildly basic conditions. The product was subsequently purified via semi-preparative High-Performance Liquid Chromatography (HPLC) to yield ^{18}F- MK6240. The identity of the radiotracer was verified through HPLC co-injection analysis, with radiochemical purity exceeding 95% and molar activity ranging from 735 to 1120 GBq/μmol.

^{11}C-PIB was synthesized following established protocols [18], utilizing the corresponding precursors. The radiochemical purity of ^{11}C-PIB was maintained above 95%, with specific activity at 50GBq/μmoL (1.48Ci/μmoL).

PET/MRI scans

PET data were acquired using a Biograph mMR hybrid PET/MRI system (Siemens Healthineers, Erlangen, Germany), comprising a whole-body PET scanner integrated with a 3.0-T MRI. This hybrid system allows for simultaneous acquisition across 127 transaxial planes, covering a 25.8 cm axial field of view, enabling full-brain imaging in a single bed position. The ^{18}F-MK6240 PET scan began 70 min post-injection of the tracer (370MBq, 4.44-5.55MBq/kg) and continued for 20 min. It was carried out simultaneously with the MRI scan, which included attenuation correction acquisition (ultra-short echo time sequence, TE1/TE2 = 0.07/2.46 ms, TR = 11.94ms, flip angle 10°, 192 slices, matrix size: 192 × 192 × 192, FOV = 300 mm × 300 mm, voxel size: 1.6 mm×1.6 mm×1.6 mm, acquisition time 1:40 min/bed position). Concurrently, structural MRI and resting-state fMRI data were acquired, as previously detailed [17]. The ^{11}C-PIB PET/MRI scan followed a similar protocol, with data collection occurring from 40 to 60 min post-injection. Static 20-minute PET data for both ^{18}F-MK6240 and ^{11}C-PIB were reconstructed into standardized uptake value (SUV) images using an ordered subset expectation maximization algorithm with three iterations, 21 subsets, a 336 × 336 matrix, and a Gaussian filter at a 4 mm full-width half-maximum (FWHM) for further analysis.

Image and data analysis

^{18}F-MK6240 PET visual classification

The visual assessment of ^{18}F-MK-6240 PET images was performed by two nuclear medicine physicians with 4 and 2 years of experience in ^{18}F-MK-6240 imaging, respectively. Image evaluation utilized 3D- T1-weighted images (T1WI) fused with PET data, reviewed in three orthogonal planes (sagittal, coronal, and transaxial) with a standardized color scale. Visual classifications were defined as follows: (1) tau negative, indicating no ^{18}F-MK6240 retention); (2) medial temporal cortex (MTC) retention, signifying retention localized to the transentorhinal, entorhinal cortex, and hippocampus); and (3) neocortical retention, characterized by retention extending beyond the MTC to include cortical regions such as the limbic system, posterior cingulate cortex (PCC), and other neocortical areas.

Inter-rater reliability was assessed using Cohen's kappa statistic. Discrepancies between the two reviewers were resolved through joint review and consensus [19]. Based on the visual classification, participants with increased intracranial ^{18}F-MK6240 uptake were categorized as Group 2, while those without significant uptake were classified as Group 1.

^{18}F-MK6240 and ^{11}C-PIB-PET image pre-processing

High-resolution T_1-weighted MRI brain images were initially segmented for brain tissue classification and spatially normalized to a custom template created from all T1 images using the SPM12 toolbox (https://www.fil.ion.ucl.ac.uk/spm/software/spm12/). The static PET images (acquired from 40 to 60 min post-injection) were co-registered to the individual T1WI. Spatial normalization to the custom template was achieved using the transformation matrix generated during the T1WI normalization process, after which all images were transformed to MNI space for further analysis.

Derivation of SUVRs

Atlas-based parcellation of PET images into regions of interest (ROIs) was conducted using the automated anatomic labeling (AAL) atlas within MNI space. Cerebellar regions were specifically positioned over cerebellar gray matter, and ROIs were established in regions with high blood flow, including the frontal cortex, medial temporal cortex, lateral temporal cortex, parietal cortex, occipital cortex, PCC, as well as the putamen and caudate. Standardized uptake value ratios (SUVRs) were calculated with cerebellar gray matter serving as the primary reference region.

Resting-state fMRI data pre-processing

Functional MRI time series were initially corrected for gradient non-linearity and head motion, with the first

six volumes discarded to ensure magnetization equilibrium and participant adaptation to the environment. Subsequent preprocessing steps involved co-registration with corresponding T1WI MR images, brain extraction, temporal filtering via a band-pass filter set at 0.01–0.1 Hz, and regression of signals from white matter and cerebrospinal fluid. Data were then normalized to MNI space, with the normalized fMRI images smoothed using a Gaussian kernel of 6 mm FWHM and resampled to a 2-mm isotropic voxel size.

Single-subject PET-measured neocortical tau deposition map

A voxel-wise general linear model (GLM) analysis was applied to ^{18}F-MK6240 SUVR maps of cognitively normal control participants, adjusting for age, gender, and education. Analysis focused exclusively on gray matter voxels. Using beta-term and residual maps derived from the GLM, a voxel wise w-score for tau deposition was computed for each patient, in alignment with the method for generating w-scores in atrophy mapping [20]. Tau deposition w-maps were subsequently binarized at a threshold of w-score > 30, signifying that the SUVR at each voxel for a given patient was 30 times the standard deviations (SD) above the mean of the control group, adjusted for demographic variables.

Table 1 Demographic and clinical characteristics of the study participants

Value	Mean (SD)			Statistics	*P*-value
	CN (*N* = 20)	Group1 (*N* = 7)	Group2 (*N* = 7)		
Age (years)	40.3 (16.9)	40.7 (15.9)	36.7 (7.4)	H = 0.1	0.94
EYO (years)	-	-16.3 (4.4)	-7.1 (6.1)	T=-3.2	0.01
APOE ε4 carriers: number (%)	-	3 (42.8%)	1 (14.3%)	$X^2 = 1.4$	0.56
PSEN1 carriers: number (%)	-	3 (42.8%)	1 (14.3%)	$X^2 = 1.4$	0.56
PSEN2 carriers: number (%)	-	2 (28.6%)	0 (0%)	$X^2 = 2.3$	0.46
APP carriers: number (%)	-	2 (28.6%)	6 (85.7%)	$X^2 = 4.7$	0.10
Female: number (%)	11 (55%)	5 (71.4%)	7 (100%)	$X^2 = 4.9$	0.11
Education (years)	15.3 (4.2)	14.6 (2.5)	15.7 (0.5)	H = 2.1	0.35
MMSE	28.4 (1.5)	27.4 (1.3)	26.6 (2.1)	H = 5.2	0.07
AVLT Trials 1–3	-	32.6 (4.1)	31.6 (4.8)	T = 48.5	0.60
AVLT Trials 4	-	13.0 (1.4)	12.4 (1.6)	T = 49.5	0.69
AVLT Trials 5	-	13.8 (1.1)	13.9 (1.1)	T = 52.5	1.00
BNT	-	27.0 (1.0)	27.9 (1.2)	T = 42.0	0.17
HAMD	-	3.0 (2.7)	2.3 (2.6)	T = 48.5	0.60
Cortical SUVR of ^{11}C-PIB	1.11 (0.07)	1.22 (0.01)	1.48 (0.19)	H = 13.4	0.001

Abbreviations: EYO, Estimated years to symptom onset; PSEN1, Presenilin 1; PSEN2, Presenilin 1; APP, amyloid precursor protein; MMSE, Mini-Mental State Examination; AVLT Trials 1–3, Auditory Verbal Learning Test Immediate recall; AVLT Trials 4, Auditory Verbal Learning Test delay recall trial; AVLT Trials 5, Auditory Verbal Learning Test recognition trial; BNT, Boston Naming Test; HAMD, Hamilton Depression Scale

PET-measured tau deposition network mapping

The AD-associated deposition network for each patient was constructed as a voxel-wise brain functional connectivity map, linked to the individual binary tau deposition maps. This involved calculating the mean blood-oxygen-level-dependent (BOLD) time course across all voxels within each subject's tau deposition map, followed by correlation with the BOLD time course at each gray matter voxel. Connectivity values were then converted to z-scores using Fisher's *r*-to-z transformation, providing standardized measures of network connectivity in association with tau pathology.

Statistics

All data analyses were conducted using SPSS, version 23.0 (IBM Corp., Chicago, IL, USA). The distribution of demographic and clinical variables was tested for normality with the Kolmogorov-Smirnov test. The Kruskal-Wallis H test was applied to assess demographic data, MMSE, and cortical SUVR of ^{11}C-PIB among the CN, Group 1, and Group 2, with statistical significance defined at $P < 0.05$. Comparisons of EYO, neuropsychological data between G1 and G2 group were performed using the Mann-Whitney U test. Fisher's Exact Test or Fisher-Freeman-Halton exact test were used for categorical measures. As for the ROI based SUVR analysis of Aβ and tau deposition, group differences between asymptotic ADAD and CN group were assessed by independent two-sample Student's *t*-tests. Additionally, the differences in SUVR of ROI between each two groups, CN, Group 1, and Group 2, were evaluated using Mann-Whitney U Test. Spearman correlation analysis was employed to examine the relationships between SUVRs in ROIs for the two tracers and between SUVRs of ROIs for each tracer and neuropsychological scores, applying Bonferroni correction ($P < 0.05$, N = total number of comparisons).

To create tau deposition network maps, voxel-wise one-sample *t*-tests (FDR corrected, $P < 0.05$) were conducted independently for Group 1 and Group 2. Differences in ^{18}F-MK6240 binding network maps between Group 1 and Group 2 were identified with voxel-wise two-sample t-tests, also FDR corrected ($P < 0.05$).

Results

Demographic and neuropsychological characteristics

Table 1 presents the clinical and neuropsychological characteristics of three groups. Among the 34 participants, no significant differences were observed in age,

gender, *APOE* ε4 carriers percentage, education level, and neurological test scores among the three groups.

Visual assessments of ^{18}F-MK6240 PET

Two readers assessed all 14 ^{18}F-MK6240 PET/MR images. The ^{18}F-MK6240 PET scans of asymptomatic FAD carriers were visually classified into three categories: tau negative (7 subjects, 50%), MTC only (6 subjects, 42.9%), and neocortex (1 subject, 7.1%). There was substantial agreement between the readers ($\kappa = 0.71$). Additional details are provided in Supplemental Table 1.

ROI based SUVR analysis of Aβ and tau deposition

Figure 1 displays SUVR images from ^{11}C-PIB and ^{18}F-MK6240 PET scans for a representative CN individual and participants carrying the ADAD mutation. Complete SUVR values for all ROIs between asymptotic ADAD carriers and CN group are provided in Supplementary Table 2. ADAD carriers demonstrated a significantly greater Aβ burden across the cortex and striatum compared to CN, although tau PET binding did not differ significantly between the groups. Supplementary Table 3 shows the analysis between each two groups. Analysis revealed that Group 1 presented elevated Aβ deposition in the frontal cortex ($P = 0.02$), lateral temporal cortex ($P = 0.01$) and putamen ($P = 0.02$) compared to CN participants, while Group 2 exhibited more extensive ^{11}C-PIB deposition, particularly across neocortical and striatal regions. Further comparison between Group 1 and Group 2 revealed significantly higher Aβ deposits in the PCC ($P = 0.02$), parietal lobe ($P = 0.03$) and striatum ($P < 0.01$) in Group 2. Figure 2 shows that Group 2 had significantly higher MK6240-PET uptake in the MTC ($P < 0.001$) and in other cortical areas ($P < 0.05$) compared to both CN and Group 1.

The relationship between the SUVRs of both tracers and neuropsychological tests

As expectation, no correlation was observed between the SUVRs in ROIs for both ^{11}C-PIB and ^{18}F-MK6240 and neuropsychological scores in asymptomatic ADAD carriers.

PET-measured tau deposition network mapping

Figure 3 illustrates tau network mapping across Group 1, Group 2, and the comparative analysis between the two groups. Group 2 exhibited enhanced rsFC in the bilateral inferior temporal cortex, PCC, precuneus, and limbic system regions when contrasted with Group 1. In contrast, Group 2 demonstrated reduced rsFC within the left medial inferior temporal cortex and fusiform gyrus in the tau network mapping (Table 2). These findings suggest differential network connectivity patterns associated with tau deposition in Group 2, reflecting distinct neural network alterations in the preclinical ADAD stage.

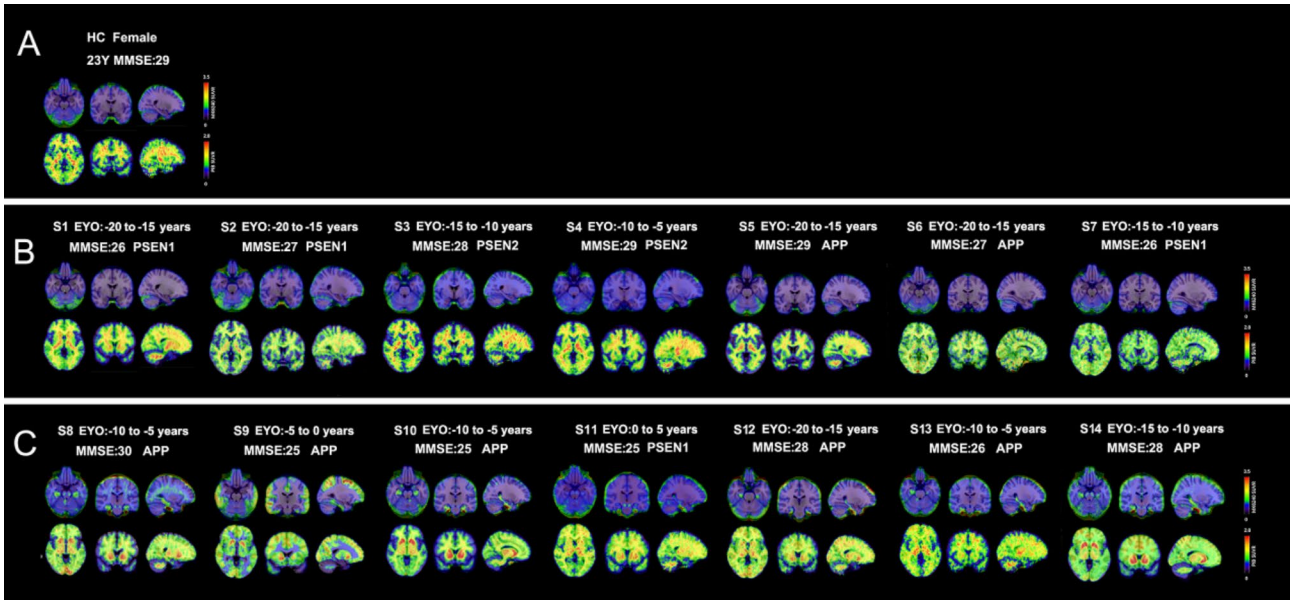

Fig. 1 Parametric SUVR images of ^{18}F-MK6240 (top row in each panel) and ^{11}C-PIB (bottom row in each panel) in a typical control case (**A**), as well as in subjects from Group 1 (**B**, $n = 7$) and Group 2 (**C**, $n = 7$). (**A**) As expectation, the dual tracer images of the CN participant showed no signs of abnormally elevated radioactivity. (**B**) For Group 1, participants demonstrated increased ^{11}C-PIB signal in the cortical and striatum regions, while no clear intracranial ^{18}F-MK6240 binding was found. (**C**) Conversely, Groups 2 participants had a significant deposition of ^{11}C-PIB across the cortex, with even more pronounced increase in the striatum. Additionally, ^{18}F-MK6240 binding was identified in the entorhinal regions, with only participant S9 showing uptake in the neocortex. The demographic details, MMSE scores and gene mutation status of subjects with familial Alzheimer's disease are illustrated

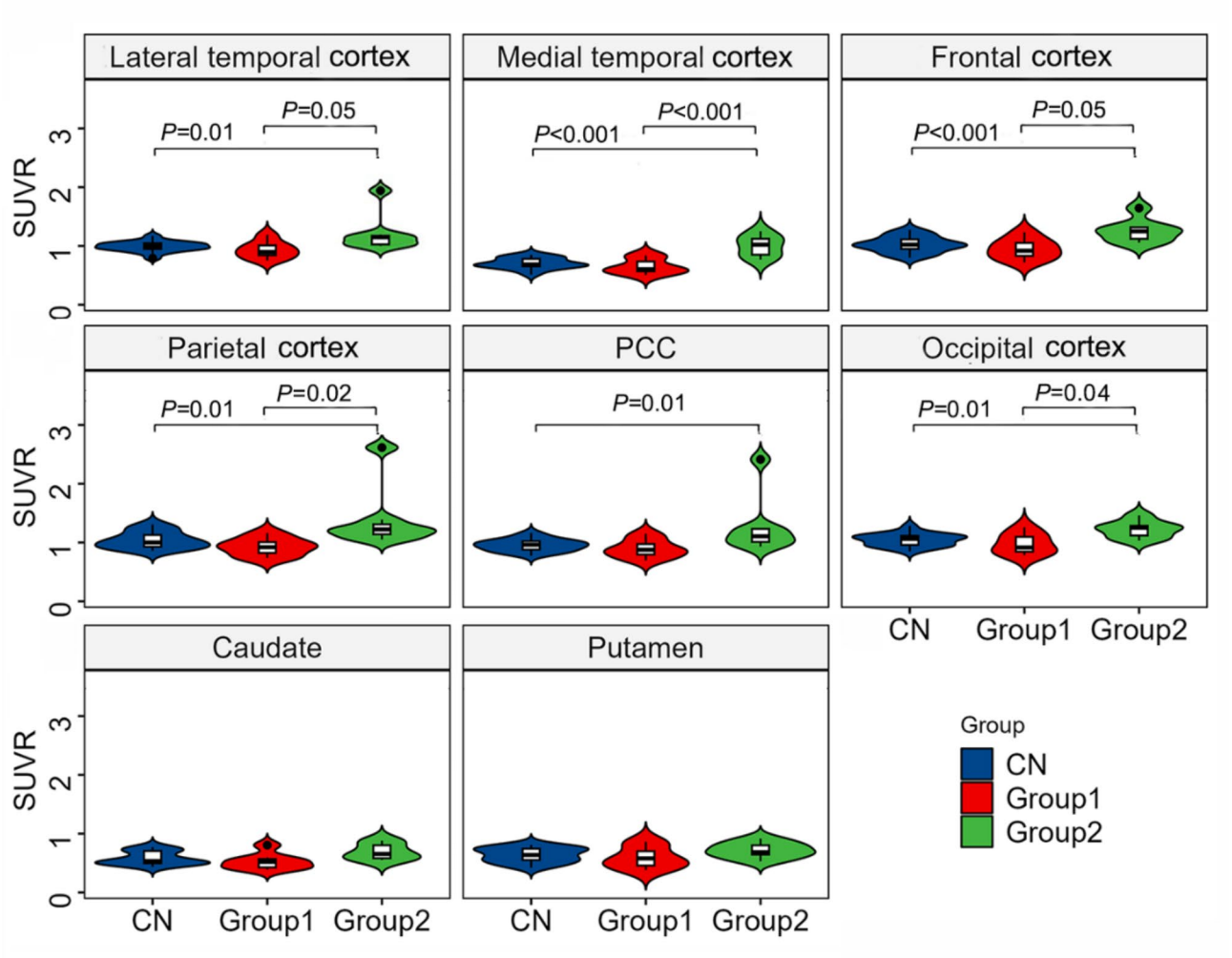

Fig. 2 ROI based SUVR analysis of ^{18}F-MK6240 in CN, Group 1 and Group 2. Group 2 exhibited a substantial increase in MK6240-PET uptake within the medial temporal cortex ($P < 0.001$) and additional cortical regions ($P < 0.05$), which was significantly greater than that observed in both the CN group and Group 1. PCC, Posterior Cingulate Cortex

Discussion

Research on asymptomatic carriers of ADAD offers a valuable window for identifying the optimal timing for intervention before irreversible neurodegeneration occurs. By leveraging PET and fMRI topographic imaging, this study investigates not only ***"when"*** but also ***"where"*** neurodegenerative processes emerge, informing potential focal points for early intervention.

Trajectories of Aβ and tau

Previous imaging studies and postmortem analyses have shown that ADAD may present distinct patterns of Aβ distribution, often displaying higher fibrillary Aβ deposition in the striatum than in the neocortex during preclinical stages, which contrasts with the patterns typically observed in sporadic AD [6–10, 21]. In alignment with these findings, our study also observed significantly elevated Aβ deposition across both cortical and striatal regions in ADAD carriers compared to healthy controls. Differences in Aβ microstructure and binding site availability, rather than overall burden or regional distribution, may account for the distinct Aβ PET binding patterns observed between ADAD and sporadic AD. Furthermore, our results suggest that Aβ in the striatum may be more strongly correlated with tau burden than Aβ deposition in the cortex, suggesting striatal Aβ as a potential marker of disease progression in preclinical ADAD [9].

Consistent with studies from the Dominantly Inherited Alzheimer Network (DIAN), our results did not show a significant difference in tau deposition between CN individuals and asymptomatic ADAD mutation carriers [11, 22]. However, it is note that the EYO of Group 2 participants was significantly shorter than that of Group 1, which is consistent with the previous reports indicating that neocortical tau deposition occurs in presymptomatic

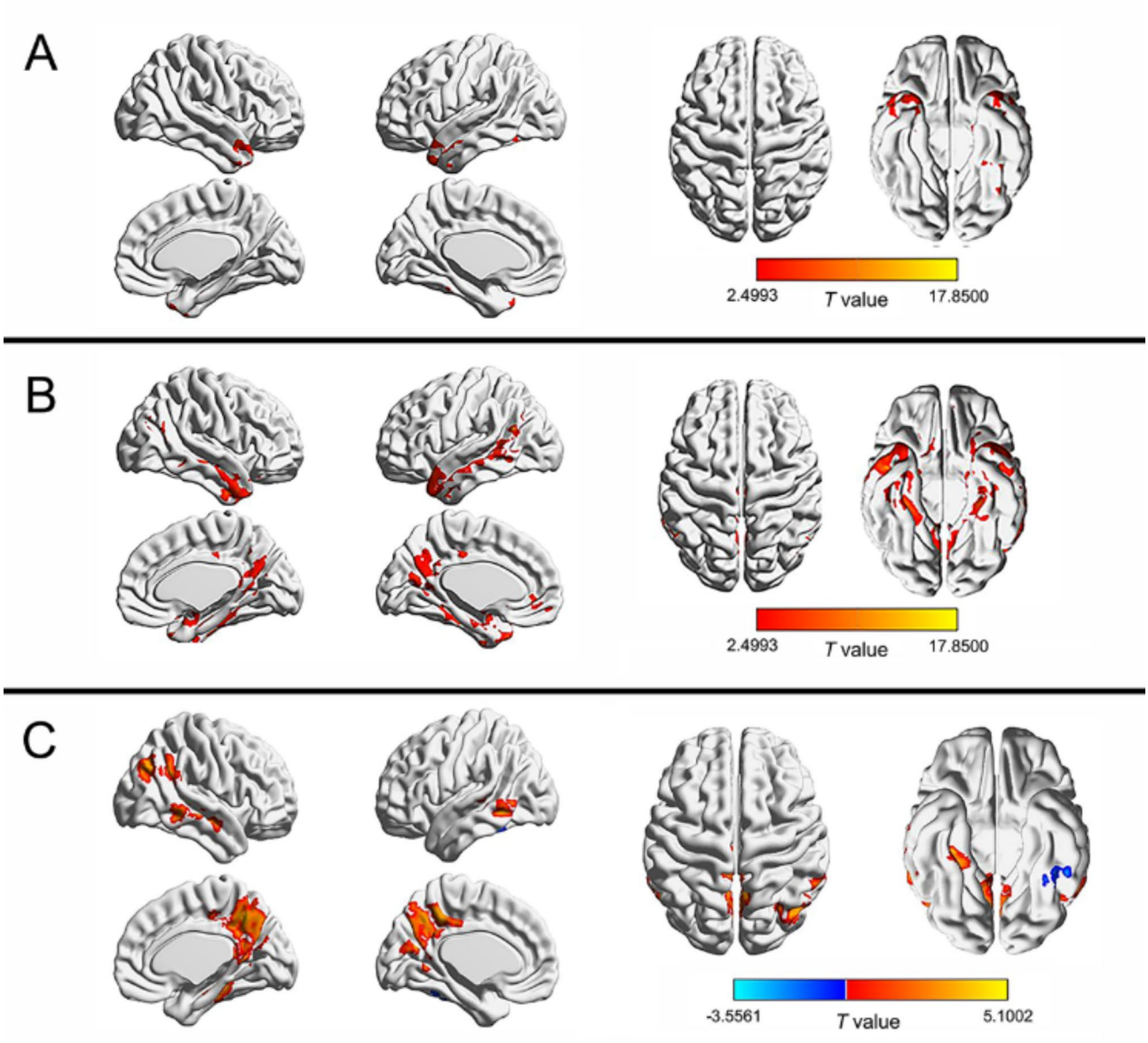

Fig. 3 The surface projection images of tau network mapping of Group 1 (**A**), Group 2 (**B**) and the comparison result between Group 2 and Group 1 (**C**). (**A**) Resting-state functional connectivity (rsFC) in bilateral basal temporal cortex was observed in the tau network mapping of Group (1) (**B**) RsFC in bilateral temporal cortex, prefrontal cortex, PCC and precuneus and lingual gyrus was shown in the tau network mapping of Group (2) (**C**) A voxel-wise *t*-test was conducted to compare tau network maps between two Groups, with voxel-wise FDR correction applied ($P < 0.05$). Enhanced rsFC was primarily noted in the posterior cortical areas and both temporal cortices, whereas a decrease in rsFC was identified in the left medial inferior temporal cortex and the fusiform gyrus

carriers nearing symptom onset [11]. In our study, Group 2 participants displayed notably increased tau levels in the entorhinal cortex, with one case showing widespread tau signal in the neocortex. A demographic analysis of this outlier, a 38-year-old APP mutation carrier with substantial Aβ and tau burdens but intact cognitive function (MMSE score of 25, CDR of 0), suggested potential cognitive resilience due to factors such as education level and protective genetic variants, such as *RELN H3447R* [23]. These findings emphasize the need for longitudinal studies to elucidate protective mechanisms that may delay clinical onset.

By categorizing subjects into two groups based on tau deposition (referred to as Group 1 and Group 2), we aimed to document the spatial and temporal interactions between Aβ and tau, a phenomenon typically captured in longitudinal studies. In this study, Group 1 represents cases where Aβ is present before tau deposition appears, whereas Group 2 includes cases where tau deposition has already manifested after Aβ build up. In this study, Group

Table 2 Altered regions of rsFC within tau-map in the comparison between Group 2 and Group 1

	No	Cluster voxels	Lateralization	Regions	T value	MNI coordinate X Y Z		
Decreased rsFC	1	85	Left	Medial inferior temporal cortex, Fusiform gyrus, BA37, BA20, BA36	-3.556	-46	-44	-24
Increased rsFC	1	2535	Bilateral	Precuneus_R, Limbic lobe, Precuneus_L, BA31, PCC, BA7, Cunues_L, Cunues_R, Calcarine_L, Calcarine_R, BA23	5.100	10	-54	46
	2	263	Right	Middle temporal gyrus, BA21, Inferior temporal gyrus	4.721	54	-36	-4
	3	239	Right	Limbic lobe, Parahippocampa gyrus, Fusiform gyrus, BA36, BA37	4.198	32	-36	-14
	4	198	Left	Middle temporal gyrus, Inferior temporal gyrus, BA37, BA22	3.701	-56	-52	-6
	5	67	Left	PCC, Limbic lobe, Precuneus, Lingual gyrus	2.935	-6	-58	10

Abbreviations: MNI, Montreal Neurosciences Institute; rsFC, resting-state functional connectivity; BA, Brodmann area; PCC, posterior cingulate cortex

1 represents cases where Aβ is present before tau deposition appears, whereas Group 2 includes cases where tau deposition has already manifested after Aβ build up. The results show that in Group 1, Aβ first deposits in the regions of putamen, LTC and frontal cortex, compared to the CN, as shown in Supplementary Table 3. This pattern suggests a progression initiated by Aβ buildup, followed by tau deposition. Although the presence of Aβ in the striatum and tau in posterior cortical regions suggests potential trajectory differences between ADAD and sporadic AD, this sequence sheds light on ADAD's natural progression, which is valuable for understanding sporadic AD etiology.

PET measured tau network mapping

In 2020, Tetreault and colleagues proposed the single-subject atrophy w-score to address individual variability in atrophy and its unique symptom patterns across patients. They also introduced "atrophy network mapping" to explore correlations between clinical, cognitive, and neuropsychiatric symptoms and specific brain networks in AD patients [20]. Previous studies have shown that single-subject variations in pathological protein deposition are also characteristic of AD [24, 25]. These approaches provide valuable insights into pathological protein buildup.

In our study, we initially analyzed rsFC between ROIs defined by the Brainnetome atlas but found no significant differences between Groups 1 and 2. We then applied the concepts of atrophy w-score and "atrophy network mapping" to develop a tau deposition w-score and a novel "tau deposition network mapping" technique. This technique enabled us to create individualized tau deposition maps and investigate potential associations between PET-identified pathology and brain function via fMRI. This approach offers several advantages over conventional ROI-based methods: First, pathology network mapping does not rely on predefined ROIs, as the pathological findings themselves define relevant regions; Second, an excess of ROIs can reduce the likelihood of detecting meaningful results. Consequently, tau network mapping serves as a complementary and potentially synergistic method alongside traditional ROI-based approaches. In sporadic AD, Luan et al. found that higher tau deposition was associated with decreased FC and worse cognitive performance with method of tau-network mapping [26]. Unlike conventional methods, network mapping, which bridges individual tau deposition maps with group-level findings, corroborates previous preclinical studies on both sporadic AD and ADAD [26–28]. Thus, this approach demonstrates how regional variability in tau deposition at the single-subject level can lead to consistent group-level neurodegeneration findings.

Schultz et al. described a "two-stage" model for AD in which Aβ and tau influence rsFC differently: initial Aβ accumulation induces increased rsFC (hyper-connectivity), which may accelerate tau spread, followed by a decline in rsFC (hypo-connectivity) as neocortical tau accumulates [27]. Our findings align with this model, as areas of variable tau deposition exhibited network-like patterns of increased rsFC in bilateral PCC, precuneus, and temporo-parietal regions, overlapping largely with the default mode network (DMN). These findings suggest a strong association between regional tau deposition and increased rsFC within the DMN in preclinical AD, emphasizing it as a potential early network marker in AD progression.

Our results also reveal reduced functional connectivity in the left medial inferior temporal cortex and fusiform gyrus, consistent with previous findings [29, 30]. Berron et al. found that elevated tau-PET signals in the transentorhinal and entorhinal regions of cognitively normal individuals were associated with decreased rsFC between the MTC and anterior temporal areas [29]. These observations also align with another study that indicates a hippocampal-anterior temporal disconnection linked to increasing MTC tau-PET signals [30]. This pattern indicates that networks vulnerable to early tau deposition may be associated with memory decline. Longitudinal studies with this cohort will be crucial to understand the

evolution of these functional connectivity networks and their relationship to clinical symptoms as tau pathology progresses.

Our research highlights tau-mediated rsFC alterations in asymptomatic ADAD mutation carriers. The most effective therapeutic window may be the "hyper-connectivity stage", suggesting that interventions such as repetitive Transcranial Magnetic Stimulation (rTMS) could be applied during this phase. Our tau network mapping approach offers a method for assessing brain disconnection at an individual level, potentially facilitating personalized rTMS targeting.

This study has some limitations. Firstly, it is a cross-sectional study with a limited number of participants; future studies should consider longitudinal research with larger samples. However, due to the rarity of asymptomatic ADAD mutation carriers, dividing them based on tau deposition helps us to observe potential changes over time. Secondly, our study group comprised participants with various mutations, including PS1 and APP. The diverse genetic mutations and pathogenic variants could lead to different clinical presentations and imaging results. Thus, further research focusing on more specific pathogenic variants among preclinical carriers of ADAD is necessary to validate the current findings.

Conclusions

Individuals with ADAD mutations provide an effective model for studying the preclinical stage of AD. Our research provides new insight about both of the "where" (the spatial distribution of pathology) and "when" (the temporal dynamics of pathological deposition, and the shifts between hyper-connectivity and hypo-connectivity) in preclinical stage of AD. The innovative tau network mapping technique holds significant potential as a novel tool for investigating the link between tauopathies and neural functional connectivity network for AD.

Abbreviations

AAL	Automated anatomic labeling
Aβ	Amyloid-beta
AD	Alzheimer's disease
ADAD	Autosomal dominant Alzheimer's disease
APP	Amyloid precursor protein
AVLT	Trials 1–3 Auditory Verbal Learning Test Immediate recall
AVLT	Trials 4 Auditory Verbal Learning Test delay recall trial
AVLT	Trials 5 Auditory Verbal Learning Test recognition trial
BA	Brodmann area
BNT	Boston Naming Test
BOLD	Blood-oxygen-level-dependent
CDR	Clinical Dementia Rating
CFAN	Chinese Familial Alzheimer's Disease Network
CN	Cognitively normal healthy volunteers
DIAN	Dominantly Inherited Alzheimer Network
DMN	Default mode network
EYO	Estimated years to symptom onset
FWHM	Full-width half-maximum
GLM	General linear model
HAMD	Hamilton Depression Scale
HPLC	High-Performance Liquid Chromatography
MMSE	Mini-Mental State Examination
MNI	Montreal Neurosciences Institute
MTC	Medial temporal cortex
PCC	Posterior cingulate cortex
PET/MRI	Positron emission tomography/magnetic resonance imaging
PSEN1/2	Presenilin 1/2
ROIs	Regions of interest
rsFC	Resting-state functional connectivity
rTMS	Repetitive Transcranial Magnetic Stimulation
SD	Standard deviations
SUV	Standardized uptake value
SUVRs	Standardized uptake value ratios
TBA-HCO_3	Tetrabutylammonium bicarbonate
T1WI	T1-weighted images

Supplementary Information

The online version contains supplementary material available at https://doi.org/10.1186/s13195-025-01690-1.

Supplementary Material 1

Acknowledgements

We want to thank Professor Jia jianping for his invaluable contributions to both the execution of the entire experiment and the composition of the article. Additionally, we extend our appreciation to EditSprings (https://www.editsprings.com/) for the expert linguistic services provided.

Author contributions

QGW, QW, CL, YDW, JG and LPF organized patient recruitment, collected clinical data and conducted neuropsychological assessments. XJZ and JJL handled the preparation and quality control of PET molecular probes, as well as data management for PET/MRI. LWL, ZZ, RMW and LPF composed the hypotheses, analyzed the data and wrote the manuscript.

Funding

This study was financially sponsored by the National Natural Science Foundation of China (No. 82071963, 82371999), the Beijing Municipal Natural Science Foundation (No. 7242128), the Health Special Research Projects (No. 24BJZ14) and the National High Level Hospital Clinical Research Funding (No. 2023-NHLHCRF-YXHZ-ZRZD-01).

Data availability

No datasets were generated or analysed during the current study.

Declarations

Ethics approval and consent to participate

This study was conducted in compliance with the principles of the Declaration of Helsinki. All participants provided informed written consent to participate in the study. The study was approved by the institutional review board of the Chinese PLA General Hospital.

Consent for publication

All authors consent to the publication of this study.

Competing interests

The authors declare no competing interests.

Author details

[1]Department of Neurology, China-Japan Friendship Hospital, Yinghua East Road Hepingli, Beijing 100029, China
[2]Innovation Center for Neurological Disorders, Department of Neurology, Xuanwu Hospital, National Clinical Research Center for Geriatric Diseases, Capital Medical University, Changchun Street 45, Beijing 100037, China
[3]Theranostics and Translational Research Center, Institute of Clinical Medicine, Peking Union Medical College Hospital, Chinese Academy of Medical Sciences & Peking Union Medical College, Dongdan Santiao 9, Beijing 100730, China

[4]Department of Nuclear Medicine, The First Medical Center of Chinese PLA General Hospital, Fuxing Road 28, Beijing 100039, China
[5]Department of Nuclear Medicine, China-Japan Friendship Hospital, Yinghua East Road Hepingli, Beijing 100029, China

Received: 26 November 2024 / Accepted: 1 February 2025
Published online: 17 February 2025

References

1. Sperling R, Mormino E, Johnson K. The evolution of preclinical Alzheimer's disease: implications for prevention trials. Neuron. 2014;84(3):608–22.
2. Ryan NS, Nicholas JM, Weston PSJ, Liang Y, Lashley T, Guerreiro R, et al. Clinical phenotype and genetic associations in autosomal dominant familial Alzheimer's disease: a case series. Lancet Neurol. 2016;15(13):1326–35.
3. Fuller JT, Cronin-Golomb A, Gatchel JR, Norton DJ, Guzmán-Vélez E, Jacobs HIL, et al. Biological and cognitive markers of Presenilin1 E280A autosomal Dominant Alzheimer's disease: a Comprehensive Review of the Colombian Kindred. J Prev Alzheimers Dis. 2019;6(2):112–20.
4. Ryman DC, Acosta-Baena N, Aisen PS, Bird T, Danek A, Fox NC, et al. Symptom onset in autosomal dominant Alzheimer disease: a systematic review and meta-analysis. Neurology. 2014;83(3):253–60.
5. Crary JF, Trojanowski JQ, Schneider JA, Abisambra JF, Abner EL, Alafuzoff I, et al. Primary age-related tauopathy (PART): a common pathology associated with human aging. Acta Neuropathol. 2014;128(6):755–66.
6. Hanseeuw BJ, Betensky RA, Mormino EC, Schultz AP, Sepulcre J, Becker JA, et al. PET staging of amyloidosis using striatum. Alzheimers Dement. 2018;14(10):1281–92.
7. Villemagne VL, Ataka S, Mizuno T, Brooks WS, Wada Y, Kondo M, et al. High striatal amyloid beta-peptide deposition across different autosomal Alzheimer disease mutation types. Arch Neurol. 2009;66(12):1537–44.
8. Cohen AD, McDade E, Christian B, Price J, Mathis C, Klunk W, et al. Early striatal amyloid deposition distinguishes Down syndrome and autosomal dominant Alzheimer's disease from late-onset amyloid deposition. Alzheimers Dement. 2018;14(6):743–50.
9. Hanseeuw BJ, Lopera F, Sperling RA, Norton DJ, Guzman-Velez E, Baena A, et al. Striatal amyloid is associated with tauopathy and memory decline in familial Alzheimer's disease. Alzheimers Res Ther. 2019;11(1):17.
10. Iaccarino L, Llibre-Guerra JJ, McDade E, Edwards L, Gordon B, Benzinger T, et al. Molecular neuroimaging in dominantly inherited versus sporadic early-onset Alzheimer's disease. Brain Commun. 2024;6(3):fcae159.
11. O'Connor A, Cash DM, Poole T, Markiewicz PJ, Fraser MR, Malone IB, et al. Tau accumulation in autosomal dominant Alzheimer's disease: a longitudinal [(18)F]flortaucipir study. Alzheimers Res Ther. 2023;15(1):99.
12. Sanchez JS, Hanseeuw BJ, Lopera F, Sperling RA, Baena A, Bocanegra Y, et al. Longitudinal amyloid and tau accumulation in autosomal dominant Alzheimer's disease: findings from the Colombia-Boston (COLBOS) biomarker study. Alzheimers Res Ther. 2021;13(1):27.
13. Jack CR Jr., Bennett DA, Blennow K, Carrillo MC, Dunn B, Haeberlein SB, et al. NIA-AA Research Framework: toward a biological definition of Alzheimer's disease. Alzheimers Dement. 2018;14(4):535–62.
14. Iaccarino L, Tammewar G, Ayakta N, Baker SL, Bejanin A, Boxer AL, et al. Local and distant relationships between amyloid, tau and neurodegeneration in Alzheimer's Disease. Neuroimage Clin. 2018;17:452–64.
15. Franzmeier N, Neitzel J, Rubinski A, Smith R, Strandberg O, Ossenkoppele R, et al. Functional brain architecture is associated with the rate of tau accumulation in Alzheimer's disease. Nat Commun. 2020;11(1):347.
16. Smith RX, Strain JF, Tanenbaum A, Fagan AM, Hassenstab J, McDade E, et al. Resting-state functional connectivity disruption as a pathological biomarker in autosomal Dominant Alzheimer Disease. Brain Connect. 2021;11(3):239–49.
17. Fu L, Zhou Z, Liu L, Zhang J, Xie H, Zhang X, et al. Functional abnormality Associated with Tau Deposition in Alzheimer's Disease - A Hybrid Positron Emission Tomography/MRI Study. Front Aging Neurosci. 2021;13:758053.
18. Philippe C, Haeusler D, Mitterhauser M, Ungersboeck J, Viernstein H, Dudczak R, et al. Optimization of the radiosynthesis of the Alzheimer tracer 2-(4-N-[11 C]methylaminophenyl)-6-hydroxybenzothiazole ([11 C]PIB). Appl Radiat Isot. 2011;69(9):1212–7.
19. Krishnadas N, Huang K, Schultz SA, Doré V, Bourgeat P, Goh AMY, et al. Visually identified tau 18F-MK6240 PET patterns in symptomatic Alzheimer's Disease. J Alzheimers Dis. 2022;88(4):1627–37.
20. Tetreault AM, Phan T, Orlando D, Lyu I, Kang H, Landman B, et al. Network localization of clinical, cognitive, and neuropsychiatric symptoms in Alzheimer's disease. Brain. 2020;143(4):1249–60.
21. Klunk WE, Price JC, Mathis CA, Tsopelas ND, Lopresti BJ, Ziolko SK, et al. Amyloid deposition begins in the striatum of presenilin-1 mutation carriers from two unrelated pedigrees. J Neurosci. 2007;27(23):6174–84.
22. Gordon BA, Blazey TM, Christensen J, Dincer A, Flores S, Keefe S, et al. Tau PET in autosomal dominant Alzheimer's disease: relationship with cognition, dementia and other biomarkers. Brain. 2019;142(4):1063–76.
23. Lopera F, Marino C, Chandrahas AS, O'Hare M, Villalba-Moreno ND, Aguillon D, et al. Resilience to autosomal dominant Alzheimer's disease in a Reelin-COLBOS heterozygous man. Nat Med. 2023;29(5):1243–52.
24. Vogel JW, Young AL, Oxtoby NP, Smith R, Ossenkoppele R, Strandberg OT, et al. Four distinct trajectories of tau deposition identified in Alzheimer's disease. Nat Med. 2021;27(5):871–81.
25. Jeon S, Kang JM, Seo S, Jeong HJ, Funck T, Lee SY, et al. Topographical heterogeneity of Alzheimer's Disease based on MR Imaging, Tau PET, and amyloid PET. Front Aging Neurosci. 2019;11:211.
26. Luan Y, Rubinski A, Biel D, Otero Svaldi D, Alonzo Higgins I, Shcherbinin S, et al. Tau-network mapping of domain-specific cognitive impairment in Alzheimer's disease. Neuroimage Clin. 2024;44:103699.
27. Schultz AP, Chhatwal JP, Hedden T, Mormino EC, Hanseeuw BJ, Sepulcre J, et al. Phases of Hyperconnectivity and Hypoconnectivity in the default Mode and Salience Networks track with amyloid and tau in clinically normal individuals. J Neurosci. 2017;37(16):4323–31.
28. Veldsman M. Atrophy network mapping of transdiagnostic cognitive and neuropsychiatric symptoms. Brain. 2020;143(4):1053–6.
29. Berron D, Vogel JW, Insel PS, Pereira JB, Xie L, Wisse LEM, et al. Early stages of tau pathology and its associations with functional connectivity, atrophy and memory. Brain. 2021;144(9):2771–83.
30. Harrison TM, Maass A, Adams JN, Du R, Baker SL, Jagust WJ. Tau deposition is associated with functional isolation of the hippocampus in aging. Nat Commun. 2019;10(1):4900.

Publisher's note